scientific reports

Check for updates

OPEN

Multiscale dynamics analysis of lumbar vertebral cortical bone based on the Abaqus submodel finite element method

Chunlei Ju[1], Kai Yang[1], Qingwei Yang[2], Yang Mi[1], Chunhong Wang[1]✉ & Hongming Ji[1]✉

The direct effect of macroscopic loads on the microstructure of bone tissue in a vibration environment is not yet known. Therefore, this study aims to investigate the macro- and micro-biomechanical properties of the lumbar spine system under dynamic loading in such an environment. We analyzed the dynamic characteristics of osteon by establishing a macro- and micro-scale model of the lumbar spine, using a submodel-specific boundary displacement method based on St. Venant's principle. Utilizing the results from the transient dynamic analysis of the entire lumbar spine as boundary conditions, this study simulates the dynamic behavior of osteon in each segment of the spine on a microscopic scale. The macroscopic results of the transient dynamic analysis showed that the rates of change in dynamic displacement amplitude relative to static displacement amplitude for the L1-L5 vertebrae were 212.60%, 242.11%, 314.80%, 1.17%, and 3.75%, respectively. The change in displacement amplitude under dynamic load relative to static load was highest for the L3 vertebra, as observed in the macroscopic model. The stress and strain values in the microscopic osteon of each lumbar spine segment under sinusoidal periodic loading were higher than those in the macroscopic osteon. In the microscopic bone unit, the maximum stress occurred at the cement line during the peak stress moment, while the minimum stress was observed at the innermost bone plate during the moment of minimum stress. Under dynamic loading, the microscopic bone osteon demonstrated a cyclic stress and strain response, with variations observed in different components of the osteon. These findings provide new insights into the biomechanical behavior of the lumbar spine in a vibration environment.

Keywords Finite element analysis, Vibration load, Dynamic response, Multiscale analysis, Submodels

People exposed to vibration for prolonged periods experience constant stretching and compression of the spine, which not only causes muscle fatigue but can also lead to damage to the surrounding soft tissues. Epidemiological studies have shown that individuals affected by vibration have a 1.4- to 9.5-fold increased risk of back pain compared to those not exposed to vibration[1–4]. The spinal tissues are subjected to stresses and strains under dynamic loading that are two to three times greater than those under static loading conditions[5]. Prolonged exposure to vibration and abnormal loading patterns on the spine can stimulate bone resorption and remodeling processes, which are governed by Wolff's law. According to Wolff's law, bone structure is dynamically adapted in response to the mechanical forces applied to it. Under repetitive vibrational and abnormal loading conditions, these forces can lead to changes in bone density and microstructure, promoting bone resorption and remodeling to accommodate the new mechanical environment[6], which in turn triggers a variety of spine-related diseases[7]. Repetitive stresses and external vibration effects not only lead to increased tissue fatigue and disc degeneration but may also exacerbate spinal deformities[8], leading to a further decline in health.

Existing studies on spine dynamics have focused on the macroscopic scale, involving experimental studies, mathematical analyses, and finite element analyses of vibration hazards and cumulative damage in the spine[9–15]. As Kong and Goel[11] suggested in their calculations, the resonance frequency decreases with the number of motion segments, and the trend of resonance frequency decreasing after the L1-S segment gradually levels off. The mass of the upper body significantly affects the resonance frequency of the lumbar spine. Studies conducted by Guo and Teo[16] showed that an increase in the mass of the upper part of the human body leads to a decrease in

[1]The Neurosurgery Department of Shanxi Provincial People's Hospital, Shanxi Medical University, Taiyuan 030012, China. [2]College of Mechanical Engineering, Xinjiang University, Urumqi 830000, Xinjiang, China. ✉email: 435517769@qq.com; hongmingj@sina.com

the resonance frequency of the T12-S1 segment. The study conducted by Fan et al.[17] revealed that by adjusting the position of the center of mass of the upper body, either by shifting it forward or backward in a standard upright sitting posture, the resonance frequency in the vertical direction can be effectively reduced through a dynamics analysis of a finite element model of the T12-pelvic region. These results have improved the understanding of the vibrational response characteristics of the human spine.

A bone unit is a microscopic component of bone structure and is one of the crucial structures at the microscopic scale. When an external force is applied to a macroscopic bone, a very detailed meshing is required to accurately calculate the stress distribution within the bone unit, greatly increasing the computational effort of finite element analysis. In recent years, the development of multiscale finite element analysis methods has made it possible to reveal the mechanical behavior of material microstructures while controlling the overall number of elements. In particular, Deligianni et al.[18] investigated the stress and deformation of osteoclastic cavities in femurs subjected to loads using a multiscale finite element method, and their analytical results were highly consistent with the experimental data. Existing studies on the micromechanical properties of bone started late and were primarily experiment-oriented. Nobakhti et al.[19] developed a series of experimental based finite element models for bovine bone micro mechanics. Considered different levels of detail in the microstructure of bones and combined them with the results of physical three-point bending tests and a composite model for analyzing individual bones. Tian et al.[20] assessed the effects of whole-body vibration on the microstructure and mechanical properties of rat bone and lumbar vertebrae before and after depopulation, including by Micro-CT scanning.

When analyzing the mechanical properties of the spine, the direct effect of macroscopic loads on the microstructure of bone tissue in a vibration environment is not yet known. This direct effect of macroscopic loading on the microstructure further leads to changes in the mechanical properties of the bone tissue, which are also manifested at the microscopic level. In the fields of medicine and engineering, it is extremely important to deeply investigate the mechanical properties of bone when subjected to dynamic loading. Especially when studying a complex multi-degree-of-freedom system such as the lumbar spine, it is necessary to analyze both the role of macroscopic loading and the microstructural level. Therefore, this study will focus on investigating the influence of microscopic biomechanical properties of the lumbar spine system in a vibration environment.

Materials and methods

Ethical approval

for this project was granted by Shanxi Provincial People's Hospital Human Subject Ethics Committee, and all research was performed in accordance with relevant guidelines and regulations. The subject was informed of the experimental procedures and gave written informed consent for participating in the CT scanning.

Macro-modeling

Volunteers for this study had detailed knowledge of the study, and their written consent was obtained. In this paper, a total of 511 DICOM images were acquired by CT from the upper edge of L1 to the sacrum with a slice spacing of 0.600 mm. Tube Voltage (kV): 120 kV; Tube Current (mA): 240 mA; Scan Slice Thickness: 0.600 mm. Based on the CT scan dataset, a 3D geometric model of the lumbar spine was obtained by isolating the target region and performing 3D reconstruction by setting a grayscale threshold and manually modifying it in Mimics 21.0 (Materialise, Belgium). The 3D model in Mimics was exported in STL format to Geomagic Studio 12.0 (Geomagic, USA) for geometric routing and surface smoothing optimization, as well as reverse engineering to build the disc contour. Mesh delineation and material property assignment of the model were performed in Hypermesh 2022 (Altair, USA), and finite element analysis calculations were conducted using Abaqus 2021 (Simulia, USA) software.

The complete nonlinear finite element model shown in Fig. 1 includes cortical bone, cancellous bone, posterior structures, intervertebral discs, endplates, and ligaments. Cortical bone and cancellous bone are considered orthotropic anisotropic materials[21]. Cortical bone thickness and endplate thickness were set to 1 mm and defined as C3D8R elements[22]. The endplate mesh was connected to the vertebral body and intervertebral disc mesh using a co-nodal approach. The intervertebral disc consists of the nucleus pulposus, the fibrous matrix, and the annulus fibrosus, with the nucleus pulposus volume accounting for about 44% of the disc volume[23]. The annulus fibrosus includes 6 layers of T3D2 elements with decreasing stiffness from lateral to medial. The ligaments included seven models: the capsular ligament (CL), intertransverse ligament (ITL), supraspinous ligament (SSL), interspinous ligament (ISL), ligamentum flavum (LF), anterior longitudinal ligament (ALL), and posterior longitudinal ligament (PLL). The ligaments were modeled as tensile-only trusses[24]. The detailed material parameters of each component were determined based on the literature[21–24], and the detailed information is provided in Table 1.

Micro-modeling

As shown in Fig. 2, a multilevel finite element model, ranging from the macroscopic scale (10^-2 m order of magnitude) to the fine scale (10^-4 m order of magnitude), was established in this study, focusing on the kinetic characterization of lumbar vertebral cortical bone. At the microscopic scale, the bone unit is mainly composed of components such as the Haversian canal, the bone plate media, and the cement line.

According to the literature[25], the number of concentric bone plates encircling the Haversian canal ranges from 4 to 20 layers, whereas the facial density of the cortical bone plate in cross-section ranges between 11 and 20 per square millimeter. In this study, based on a statistical sample analysis[19], we defined a single bone unit as having six layers of concentric bone plates, with a surface density set at 16 per mm^2. Specific dimensional parameters included a bone unit diameter of 200 μm, a Haversian canal diameter of 60 μm, a thickness of 10 μm for the concentric bone plates, 1 μm for the bone plate media, and 5 μm for the bonding wires. The material parameters of each structure of the bone unit are shown in Table 2[19,25].

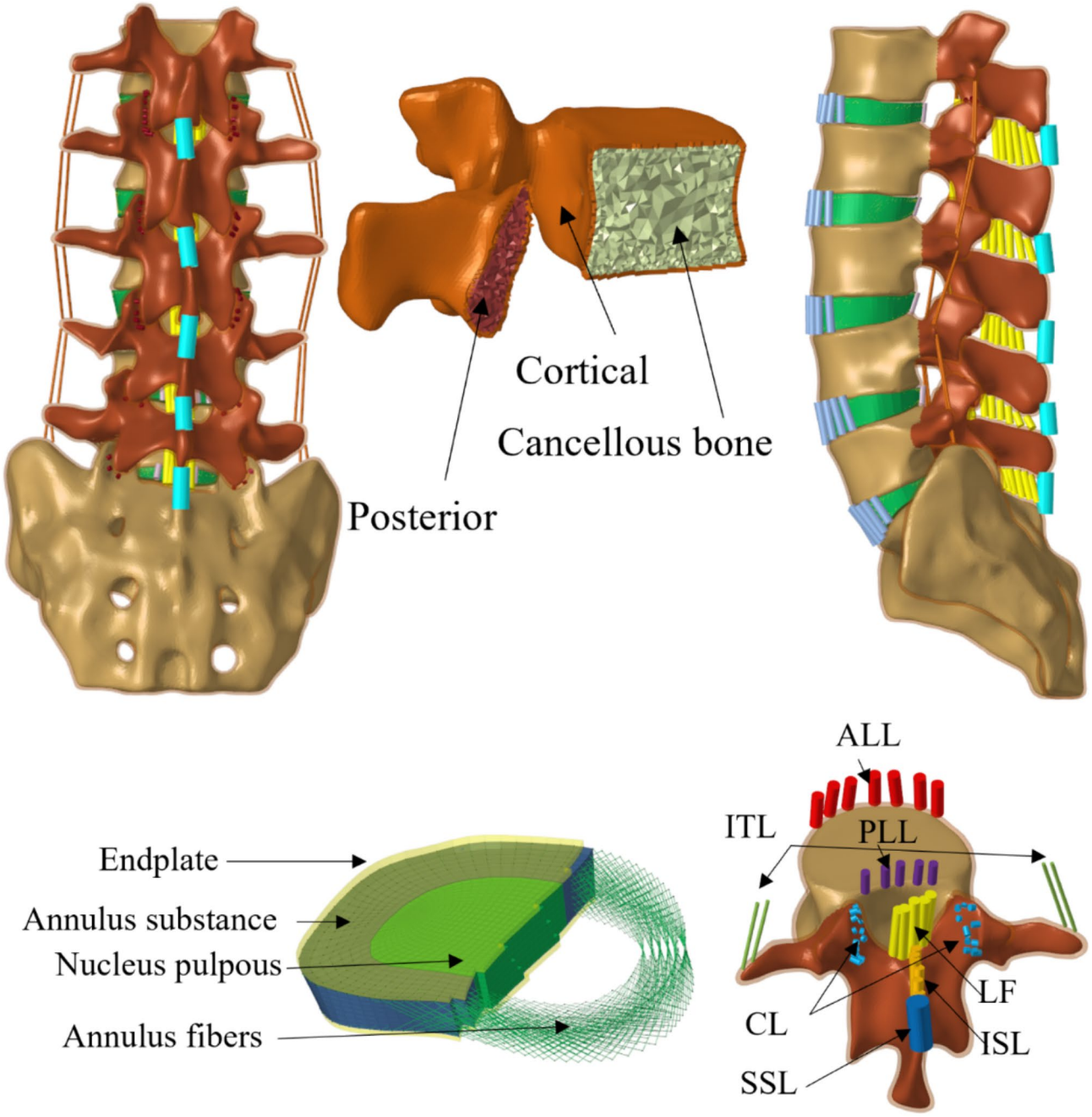

Fig. 1. Macroscopic finite element model of the lumbar spine.

Boundary conditions and contact settings

In this study, a finite element model of the human lumbar vertebrae L1-S1 was developed for further analysis. A 40 kg mass point was added to the upper surface of the vertebra at the top of the model to simulate the upper body mass of the human body[26]. Additionally, a following load of 400 N was added through temperature-coupled trusses on each side of each vertebral body, equivalent to a 200 N load on each side. The equivalent damping ratio used for transient analysis was 0.08, based on modal analysis. Briefly, all degrees of freedom of the lower surface of the sacral vertebrae were fixed, and a sinusoidal axial force of 40 N was applied to the upper surface of the vertebra at a frequency of 5 Hz[27,28].

For the boundary conditions of the microscopic bone unit model, this paper uses the submodel-specific boundary displacement method based on St. Venant's principle. The macroscopic finite element model of the human lumbar spine (L1-S1) is taken as the overall model, and the bone unit is considered a sub-model within the whole. The simulation results of the L1-S1 finite element model are used as the loads and boundary conditions for the fine-scale bone unit model of cortical bone.

Spinal components	Young's modulus (MPa)	Poisson's ratio	Cross-sectional area (mm^2)	Element type	Number of elements	Density ($10^{-6} kg/mm^3$)
Cortical	$E_{xx} = 11,300$ $E_{yy} = 11,300$ $E_{zz} = 22,000$ $G_{xy} = 3800$ $G_{yz} = 5400$ $G_{xz} = 5400$	$\upsilon_{xy} = 0.484$ $\upsilon_{yz} = 0.203$ $\upsilon_{xz} = 0.203$		C3D8R	310,324	1.7
Cancellous bone	$E_{xx} = 140$ $E_{yy} = 140$ $E_{zz} = 200$ $G_{xy} = 48.3$ $G_{yz} = 48.3$ $G_{xz} = 48.3$	$\upsilon_{xy} = 0.450$ $\upsilon_{yz} = 0.315$ $\upsilon_{xz} = 0.315$		C3D4/C3D5	849,078	1.1
Posterior	3500	0.25		C3D4	450,086	1.4
Endplate	24	0.4		C3D8R	10,538	1.2
Nucleus pulpous	C10 = 0.12, C01 = 0.03			C3D8RH	22,108	1.02
Annulus substance	C10 = 0.18, C01 = 0.045			C3D8RH	28,478	1.05
Annulus fibers Outermost layer Second layer Third layer Fourth layer Fifth layer Innermost layer	550 495 440 420 385 360	0.3 0.3 0.3 0.3 0.3 0.3	0.7 0.63 0.55 0.49 0.41 0.30	T3D2	4654	1 1 1 1 1 1
ALL	15		63.7	T3D2	35	1
PLL	18		20	T3D2	25	1
LF	12		40	T3D2	24	1
SSL	10		30	T3D2	5	1
ISL	10		40	T3D2	30	1
ITL	50		1.8	T3D2	20	1
CL	18		30	T3D2	81	1

Table 1. Material properties of the spinal components.

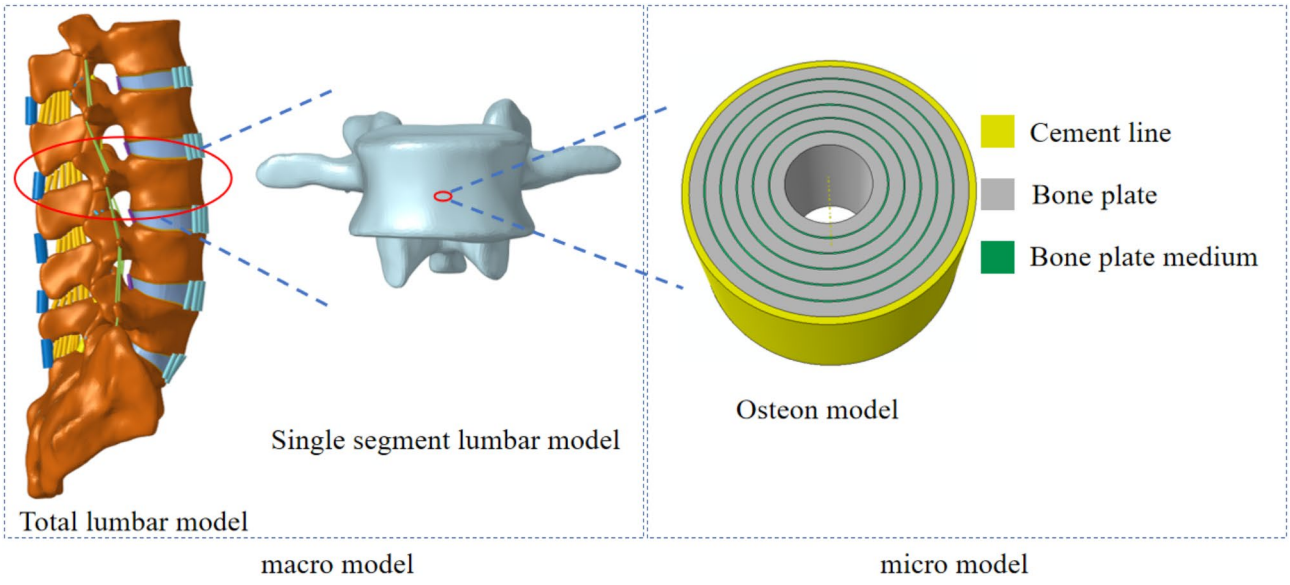

Fig. 2. The macro model (left) and micro model (right) for the lumbar spine system.

Results

Model validation results

As shown in Table 3, the first-order resonance frequencies in the vertical direction of different vertebral segment finite element models (L3-L4, L3-L5, and L1-L5) computed in this study are compared with results from the literature. The first-order vertical resonance frequencies predicted in this study are very similar to those predicted by the model in the reference[29], indicating that the model can be used to study the dynamic properties of the human body.

Composition	Unit type	Modulus of elasticity /MPa	Poisson's ratio
Bone plate	C3D8R	21,500	0.30
Bone plate medium	C3D8R	120	0.30
Cement line	C3D8R	6850	0.49

Table 2. Unit types and material parameters for each part of the bone unit.

Model segment	Results of this study(Hz)	Reference results(Hz)	Marginal notes
L3-L4	29.6	28.1	40 kg human upper body mass
L3-L5	22.7	19.6	40 kg human upper body mass
L1-L5	10.0	9.6	40 kg human upper body mass

Table 3. Comparison of results of this paper and reference.

Element sizes	L4-L5 disc pressure (MPa)	Deviation
0.8 mm	0.321	0%
1.0 mm	0.317	1.2%
1.2 mm	0.312	2.6%

Table 4. Grid independence verification.

Dynamic response	Vertebrae	Static calculation			Dynamic calculation			Rate of change
		-40 N (mm)	40 N (mm)	Change amplitude (mm)	Maximum values (mm)	Minimum value (mm)	Amplitude of vibration(mm)	
Vertebral body axial displacement (mm)	L1	0.212	-0.177	0.389	0.602	-0.614	1.216	212.60%
	L2	0.179	-0.144	0.323	0.550	-0.555	1.105	242.11%
	L3	0.112	-0.084	0.196	0.408	-0.405	0.813	314.80%
	L4	0.205	-0.224	0.429	0.197	-0.237	0.434	1.17%
	L5	0.182	-0.165	0.347	0.163	-0.197	0.36	3.75%

Table 5. The maximum and minimum values of dynamic response under the sinusoidalaxial load and comparison with the corresponding results for the static load cases.

To eliminate the influence of mesh resolution on the results, the mesh independence of the detailed lumbar spine finite element model was analyzed. For the detailed lumbar spine model, three models with different mesh sizes were developed: 1.2 mm, 1 mm, and 0.8 mm. As shown in Table 4, the deviation in the verification results did not exceed 3.0%. Ultimately, the model with a mesh size of 1.0 mm was selected.

Macro bone unit calculation results

Table 5 presents the maximum, minimum, and vibration amplitudes of the dynamic response curves, along with the corresponding static analysis results. To reflect the effect of the applied vibration load on the lumbar spine, the rate of change of the dynamic results relative to the static results is also provided in Table 5. For example, the maximum (minimum) values of the axial displacements of vertebrae L1 to L5 under sinusoidal axial vibration loads were 0.602 (-0.614) mm, 0.550 (-0.555) mm, 0.408 (-0.405) mm, 0.197 (-0.237) mm, and 0.163 (-0.197) mm, with their corresponding static analysis results being 0.212 (-0.177) mm, 0.179 (-0.144) mm, 0.112 (-0.084) mm, 0.205 (-0.224) mm, and 0.182 (-0.165) mm, respectively.

Microcosmic bone unit calculation results

The stress response of the osteon in each segment of the lumbar spine was quantitatively analyzed at both the macro and micro scales. As shown in Figs. 3, 4, 5, 6 and 7, the stress and strain-time curves of the osteon of different lumbar vertebrae exhibit cyclic changes in stress and strain under cyclic loading. The results indicate that the stress and strain values of the microscopic osteon in each segment of the lumbar spine under sinusoidal cyclic loading are larger than those of the macroscopic osteon. For example, in Fig. 4, the maximum von Mises stress values of the macroscopic osteon (Fig. 4a) for L1 to L5 are 0.34, 0.24, 0.19, 0.20, and 0.29 MPa, respectively. For the microscopic osteon (Fig. 4b), the maximum von Mises stress values for L1 to L5 are 5.52, 1.57, 1.36, 0.77, and 1.46 MPa, respectively.

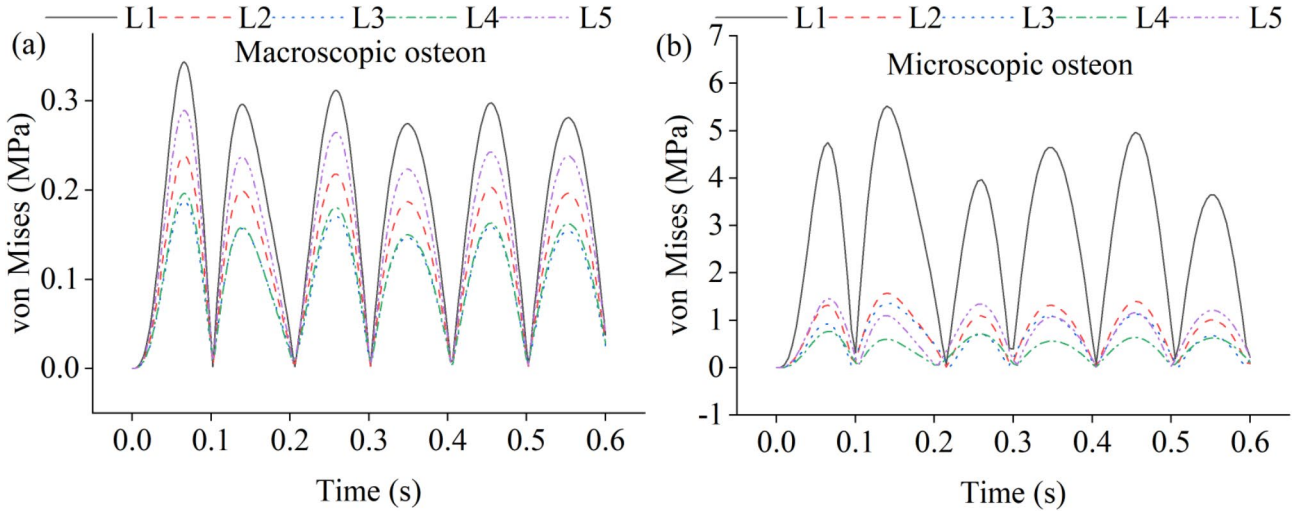

Fig. 3. Dynamic von Mises Stress Response in Macro/Micro Osteon; (**a**) Macroscopic Osteon, (**b**) Microscopic Osteon.

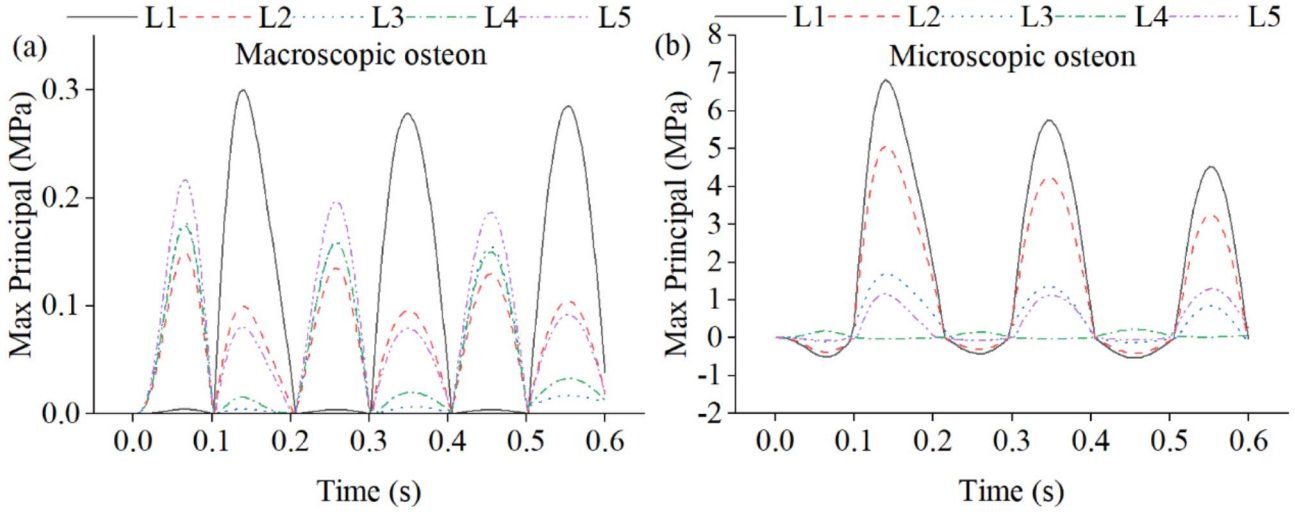

Fig. 4. Dynamic Maximum Principal Stress Response in Macro/Micro Osteon; (**a**) Macroscopic Osteon, (**b**) Microscopic Osteon.

As shown in Fig. 8, at the moment of maximum stress, the von Mises stress, maximum, and minimum principal stress values of the microscopic osteon all decrease sequentially from L1 to L4, and the stress values of the L5 vertebral osteon are slightly larger than those of the L4 vertebrae. As shown in Fig. 9, the cloud diagram demonstrates that the outermost bone plate, located inside the cement line, was subjected to the greatest stresses, and the strains were greater in the bone plate medium, with the outermost bone dplate medium having the greatest strain values.

As shown in Fig. 10, the micro-scale stress cloud used in this study clearly shows the stress-strain distribution characteristics of the vertebral osteon. The von Mises stress, maximum, and minimum stress values are largest at the innermost bone plate of the bone unit at the moment corresponding to the minimum stress value. The strain values are still larger at the bone plate medium, with the largest strain values at the outermost bone plate medium.

Discussion

In this study, the dynamic characteristics of the osteon were analyzed using a normal human lumbar spine macro-micro model based on the submodel-specific boundary displacement method derived from St. Venant's principle. By using the results of the transient dynamics analysis of the full lumbar spine with a laterally convex curvature as boundary conditions, this study simulates the dynamic behavior of the osteon of each segment of the spine on a microscopic scale. The approach we used applies the displacement results from the macro model

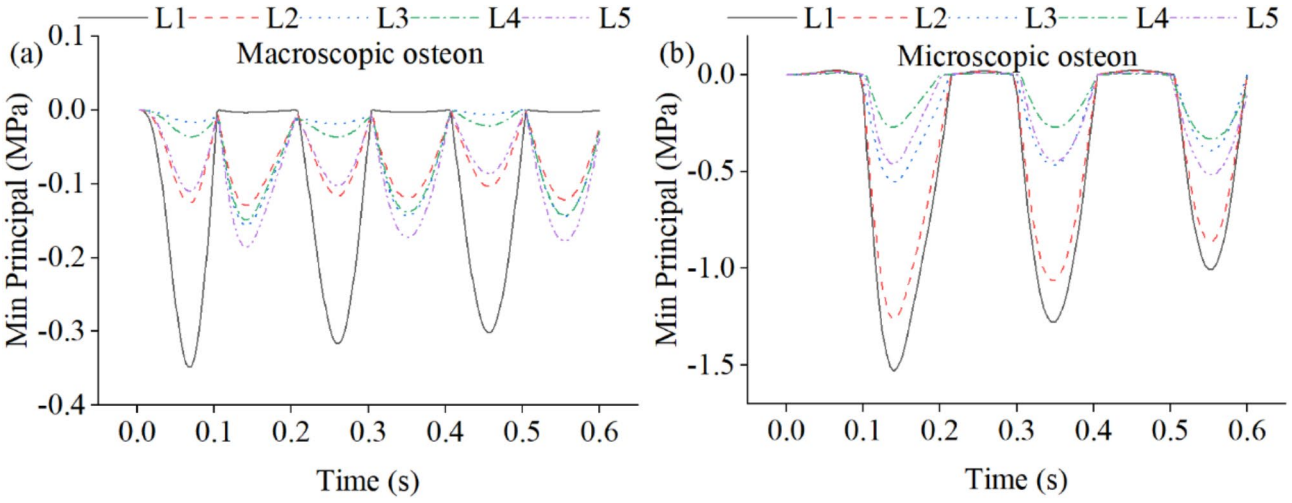

Fig. 5. Dynamic Minimum Principal Stress Response in Macro/Micro Osteon; (**a**) Macroscopic Osteon, (**b**) Microscopic Osteon.

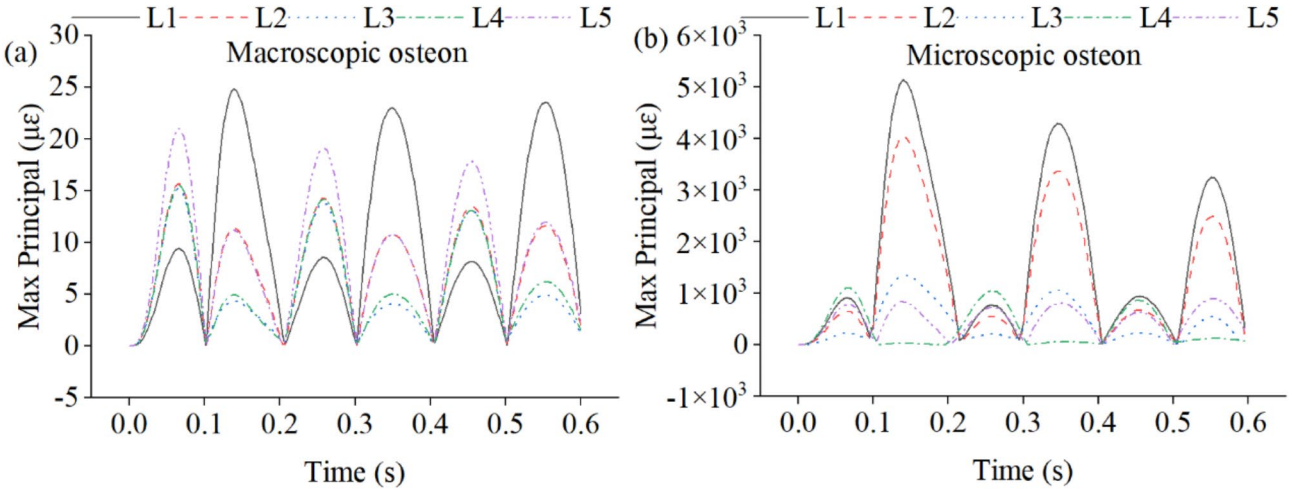

Fig. 6. Dynamic Maximum Principal Strain Response in Macro/Micro Osteon; (**a**) Macroscopic Osteon, (**b**) Microscopic Osteon.

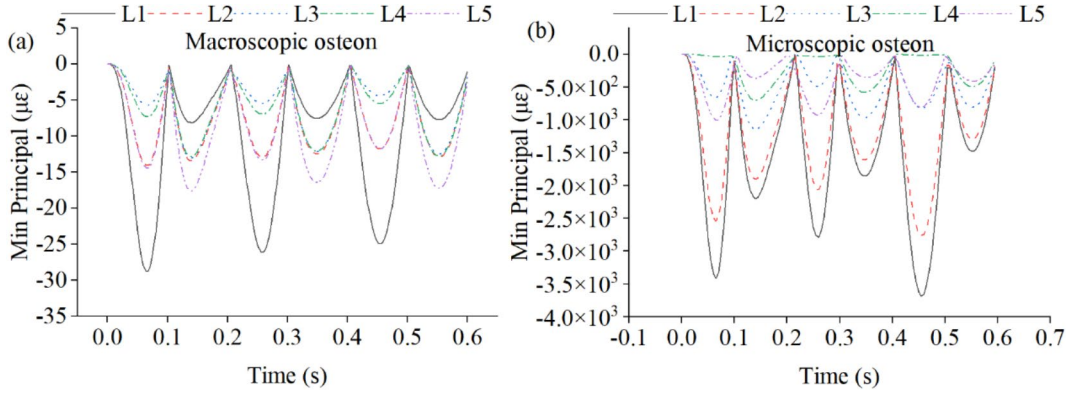

Fig. 7. Dynamic Minimum Principal Strain Response in Macro/Micro Osteon; (**a**) Macroscopic Osteon, (**b**) Microscopic Osteon.

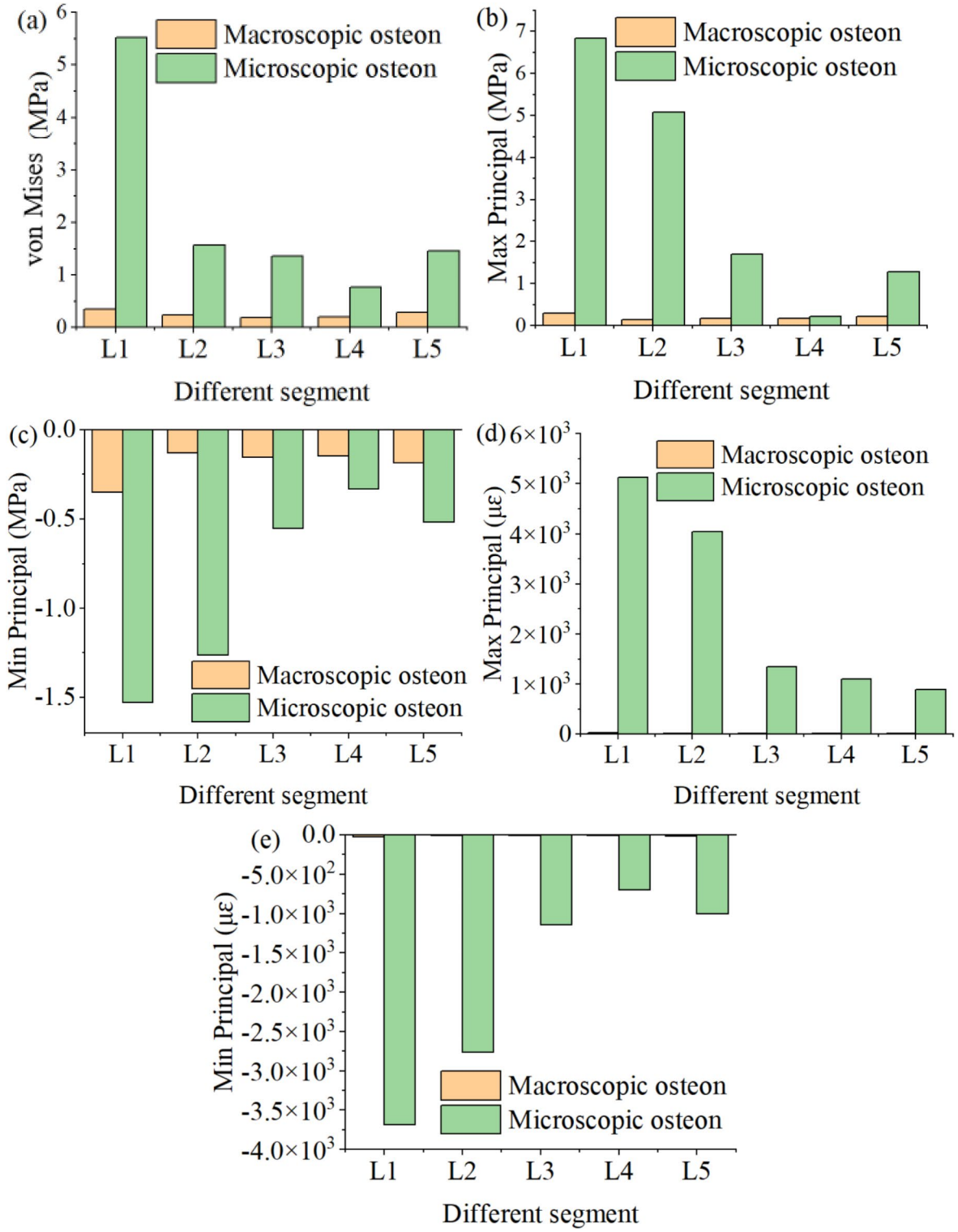

Fig. 8. Dynamic Stress and Strain Response in Macro/Micro Osteon; (**a**) von Mises Stress, (**b**) maximum Principal Stress, (**c**) minimum Principal Stress, (**d**) maximum Principal Strain, (**e**) Minimum Principal Strain.

as boundary conditions for the micro model. This ensures that the local bone unit structure under dynamic loading is accurately simulated, while maintaining the integrity of the global load transfer.

Under the same dynamic loading, the stress-strain curves of lumbar cortical bone at both the macro and micro scales exhibited cyclic responses, with the stress and strain of the micro-cortical bone being greater than those at the macro scale. This increase in stress is due to the different material properties of each part of the bone unit. Compared with the macroscopic cortical bone with homogeneous properties, the Young's modulus of the

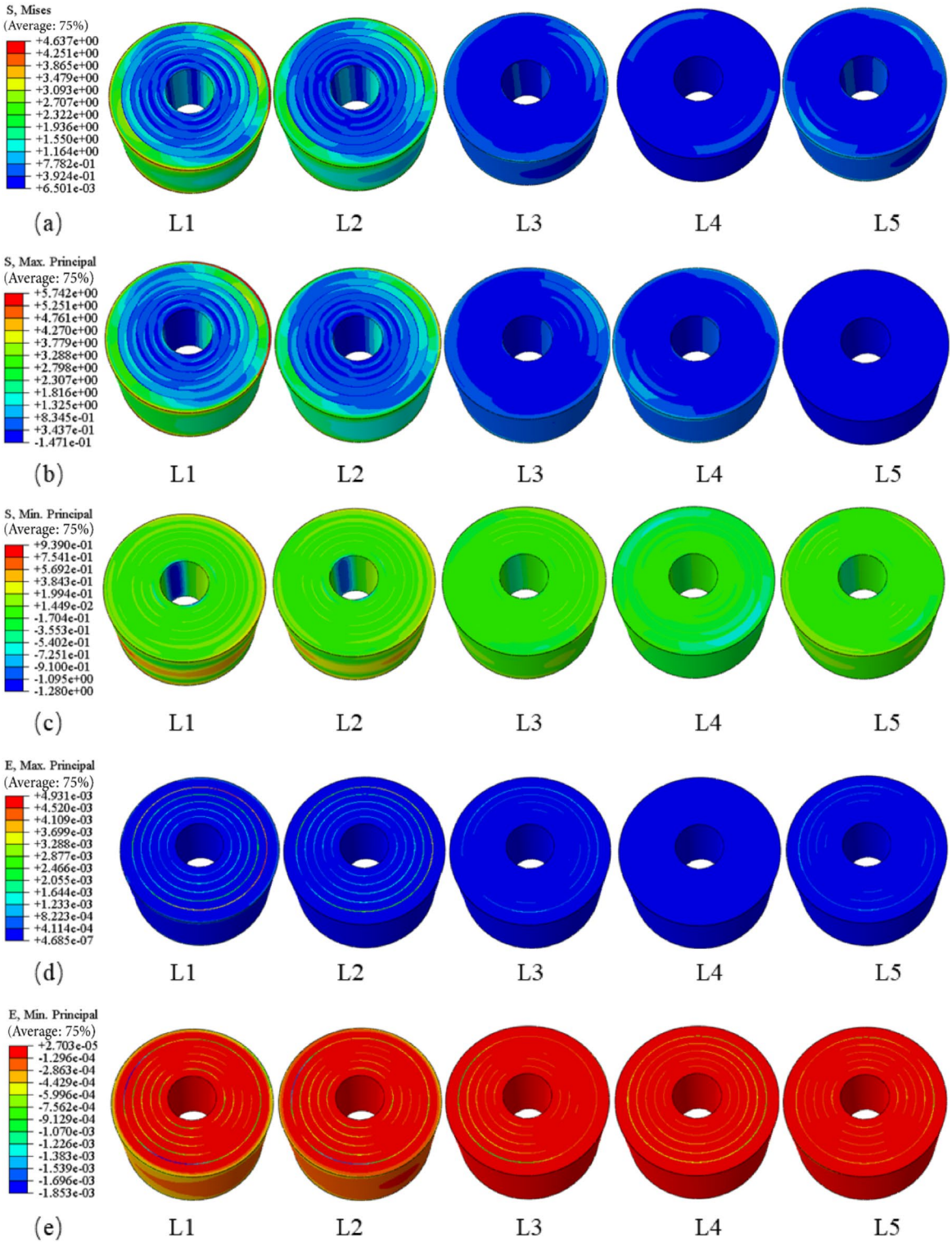

Fig. 9. Maximum Stress and Strain in Micro Osteon; (**a**) von Mises Stress, (**b**) maximum Principal Stress, (**c**) minimum Principal Stress, (**d**) maximum Principal Strain, (**e**) minimum Principal Strain.

bone plate is higher than that of the cortical bone, while the cement line and the mediator portion of the bone plate are lower than that of the cortical bone. Under the same boundary conditions, the Young's modulus was positively correlated with the stress. The stress maxima of the osteon were found in the concentric bone plates, with most of them located in the innermost bone plates near the Haversian canal.

The macroscopic calculation results showed that the osteon of each segment of the lumbar spine exhibited different displacement distribution patterns under dynamic loading. For the L3 vertebrae under a 5 Hz sinusoidal

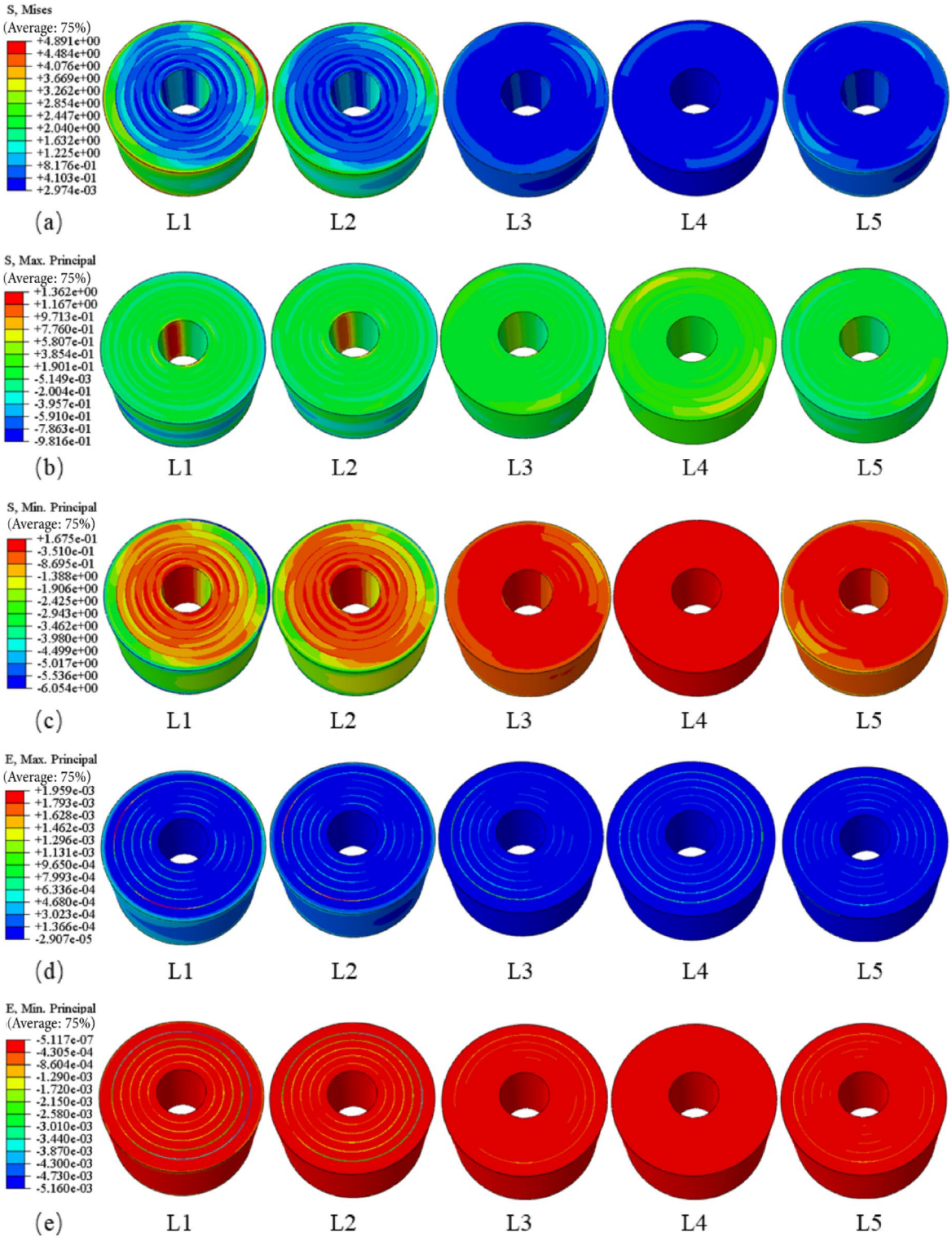

Fig. 10. Minimum Stress and Strain in Micro Osteon; (**a**) von Mises Stress, (**b**) maximum Principal Stress, (**c**) minimum Principal Stress, (**d**) maximum Principal Strain, (**e**) minimum Principal Strain.

dynamic load, the maximum and minimum displacements were 0.408 mm and −0.405 mm, respectively, compared to the corresponding maximum and minimum values under static load of 0.114 mm and −0.084 mm, respectively. under dynamic loading, the system experiences oscillations that lead to larger displacement amplitudes, whereas the static load results in more stable, smaller displacements. This difference in displacement magnitudes is mainly attributed to the dynamic effects, which produce larger oscillation amplitudes compared to the static loading scenario.The amplitude of displacement change of the L3 vertebrae under dynamic load

relative to static load was the largest, at 314.80%. These findings align with Keller's study[5], which showed that spinal tissues are subjected to stresses and strains under dynamic loading that are two to three times greater than those under static loading conditions.The results of the study showed that the dynamic responses of the lumbar spine segments under external vibratory loading were not uniform, indicating that segments with larger response results are at a higher risk of injury. Additionally, the results demonstrated that dynamic loading significantly increased the vibration amplitude of stress and strain in lumbar spine tissues compared to the corresponding static loading. This suggests that dynamic loading is more dangerous than static loading with equivalent amplitudes for the entire lumbar spine system.

In the microscopic bone unit, the time-domain results of stresses show that the moments corresponding to the stress maxima occur at the outermost bone plate. There is a certain degree of stress concentration in the cement line and part of the bone plate. At the moment corresponding to the minimum value of stress, the maximum stress occurs in the innermost bone plate. Under the same boundary conditions, the uneven distribution of material properties is more likely to cause stress concentration. According to Wolff's law, bone grows where it is needed and resorbs where it is not needed. The high-stress region of the bone unit promotes the transformation of bone cytotrophoblasts to osteoblasts, which increases the density and stiffness of the bone in this region. The stress in the bone plate medium and the cement line is significantly reduced compared to the bone plate, and this stress interruption phenomenon has a positive effect on the self-protection of the bone tissue.

Understanding the specific stress distribution and displacement patterns in different segments of the lumbar spine under dynamic loading can help in designing personalized vibration therapy protocols. By tailoring the frequency and amplitude of vibrations to the patient's specific bone characteristics, it is possible to optimize the therapeutic effects and improve treatment outcomes for individuals with osteoporosis.

There are some limitations in this study. In the macroscopic scale model, the main focus is on the overall structure of the spine, excluding the effects of soft tissues such as muscles and skin. In the micro-scale model of the bone unit, although it focuses on the internal structure of the bone, it does not cover finer structures such as the interosseous plate and bone lacunae. While simplifying the model and reducing the amount of computation, this approach may overlook the influence of certain details on the behavior of the spine. While our model provides valuable insights into the dynamic characteristics of osteon using a macro-micro approach, it lacks the detailed structural arrangement from nano- to micro-scale[30]. Future model development needs to incorporate details at different scales to improve the comprehensiveness and accuracy of biomechanical analysis.

Conclusion

In summary, we obtained the following conclusions: First, Compared with static loading, dynamic loading exerted a significantly greater influence on the magnitude of displacement change in the L3 vertebrae. Under static loading, the displacement values were smaller and more stable, indicating a less pronounced response compared to the dynamic loading case, where larger displacement amplitudes were observed due to the cyclical nature of the dynamic forces. Second, under dynamic loading, the microscopic bone unit exhibited a cyclic response pattern of stress and strain. Finally, when the stress reached its maximum value, the peak stress of the microscopic bone unit appeared at the cement line, whereas at the minimum stress, the peak stress of the microscopic bone unit was located at the innermost bone plate.These conclusions can help refine treatment protocols, including low-intensity vibration therapy, for improving bone density and preventing fractures in osteoporotic patients.

Data availability

The datasets used and/or analysed during the current study available from the corresponding author on reasonable request.

Received: 19 October 2024; Accepted: 24 February 2025
Published online: 26 February 2025

References

1. Cordover, A. M., Betz, R. R., Clements, D. H. I. & Bosacco, S. J. Natural history of adolescent thoracolumbar and lumbar idiopathic scoliosis into adulthood. *J. Spinal Disord.* **10** (3), 193–196 (1997).
2. Haefeli, M., Elfering, A., Kilian, R., Min, K. & Boos, N. Nonoperative treatment for adolescent idiopathic scoliosis: A 10- to 60-year follow-up with special reference to health-related quality of life. *Spine* **31**, 355–366 (2006).
3. Jia, S. et al. The influence of the rib cage on the static and dynamic stability responses of the scoliotic spine. *Sci. Rep.* **10**, 16916 (2020).
4. Bongers, P. M. et al. Back pain and exposure to whole body vibration in helicopter pilots. *Ergonomics* **338**, 1007–1026 (1990).
5. Keller, T. S., Colloca, C. J. & Béliveau, J. G. Force-deformation response of the lumbar spine: a sagittal plane model of posteroanterior manipulation and mobilization. *Clin. Biomech.*. **17** (3), 185–196 (2002).
6. Wolff, J. Das gesetz der transformation der Knochen. *Dtsch. Med. Wochenschr.* **19**, 1222–1224 (1893).
7. Le, P., Solomonow, M., Zhou, B. H., Lu, Y. & Patel, V. Cyclic load magnitude is a risk factor for a cumulative lower back disorder. *J. Occup. Environ. Med.* **49**, 375–387 (2007).
8. Stehbens, W. E. Pathogenesis of idiopathic scoliosis revisited. *Exp. Mol. Pathol.* **74**, 49–60 (2003).
9. Kasra, M., Shirazi-Adl, A. & Drouin, G. Dynamics of human lumbar intervertebral joints. Experimental and finite-element investigations. *Spine (Phila Pa. 1976)*. **17**, 93–102 (1992).
10. Seidel, H., Blüthner, R. & Hinz, B. Application of finite-element models to predict forces acting on the lumbar spine during whole-body vibration. *Clin. Biomech.*. **16** (Suppl 1), S57–63 (2001).
11. Kong, W. Z. & Goel, V. K. Ability of the finite element models to predict response of the human spine to sinusoidal vertical vibration. *Spine* **28**, 1961–1967 (2003).
12. Guo, L. X., Teo, E. C., Lee, K. K. & Zhang, Q. H. Vibration characteristics of the human spine under axial Cyclic loads: Effect of frequency and damping. *Spine (Phila Pa. 1976)*. **30**, 631–637 (2005).

13. Bazrgari, B., Shirazi-Adl, A. & Kasra, M. Seated whole body vibrations with high-magnitude accelerations–relative roles of inertia and muscle forces. *J. Biomech.* **41**, 2639–2646 (2008).
14. Kawchuk, G. N., Decker, C., Dolan, R., Fernando, N. & Carey, J. The feasibility of vibration as a tool to assess spinal integrity. *J. Biomech.* **41**, 2319–2323 (2008).
15. Guo, L. X. et al. Material property sensitivity analysis on resonant frequency characteristics of the human spine. *J. Appl. Biomech.* **25**, 64–72 (2009).
16. Guo, L. X. & Teo, E. C. Prediction of the modal characteristics of the human spine at resonant frequency using finite element models. *Proc. Inst. Mech. Eng. H.* **219**, 277–284 (2005).
17. Fan, W., Zhao, D. & Guo, L. X. A finite element model of the human lower thorax to pelvis spinal segment: Validation and modal analysis. *Biomed. Mater. Eng.* **32**, 267–279 (2021).
18. Deligianni, D. D. & Apostolopoulos, C. A. Multilevel finite element modeling for the prediction of local cellular deformation in bone. *Biomech. Model. Mechanobiol.* **7**, 151–159 (2008).
19. Nobakhti, S., Limbert, G. & Thurner, P. J. Cement lines and interlamellar areas in compact bone as strain amplifiers - contributors to elasticity, fracture toughness and mechanotransduction. *J. Mech. Behav. Biomed. Mater.* **29**, 235–251 (2014).
20. Tian, S., Gao, J., Gong, H., Zhang, X. & Wang, S. Effects of whole-body vibration at different periods on lumbar vertebrae in female rats. *Med. Eng. Phys.* **110**, 103918 (2022).
21. Schmidt, H. et al. Application of a calibration method provides more realistic results for a finite element model of a lumbar spinal segment. *Clin. Biomech. (Bristol Avon).* **22**, 377–384 (2007).
22. Li, Y., Zhang, Y., Xu, P., Zheng, J. & Fan, Y. Biomechanics of brain tissue damage caused by fiber endoscope penetration in third ventriculostomy surgery. *Comput. Methods Biomech. Biomed. Engin*, 27(13), 1793-1803. (2023).
23. White, A. A. & Panjabi, M. M. Clinical Biomechanics of the Spine, (1978).
24. Polikeit, A., Ferguson, S. J., Nolte, L. P. & Orr, T. E. Factors influencing stresses in the lumbar spine after the insertion of intervertebral cages: Finite element analysis. *Eur. Spine J.* **12**, 413–420 (2003).
25. Wu, L., Zou, S., Liu, R. & Zeng, Y. Bio-safety of 3D printed titanium and titanium alloys for medical application. *J. Clin. Rehabil. Tissue Eng. Res.* **22**, 5559–5564 (2018).
26. Shirazi-Adl, A. & Parnianpour, M. Role of posture in mechanics of the lumbar spine in compression. *J. Spinal Disord.*. **9**, 277–286 (1996).
27. Wilder, D. G., Woodworth, B. B., Frymoyer, J. W. & Pope, M. H. Vibration and the human spine. *Spine (Phila Pa. 1976).* **7**, 243–254 (1982).
28. Guo, L. X. & Li, W. J. Finite element modeling and Static/dynamic validation of thoracolumbar-pelvic segment. *Comput. Methods Biomech. Biomed. Engin.* **23**, 69–80 (2020).
29. Dong, R. C. & Guo, L. X. Human body modeling method to simulate the biodynamic characteristics of spine in vivo with different sitting postures. *Int. J. Numer. Method Biomed. Eng.* 33(11), (2017).
30. Gaziano, P., Monaldo, E., Falcinelli, C. & Vairo, G. Elasto-damage mechanics of osteons: A bottom-up multiscale approach. (2022).

Acknowledgements

This research did not receive any specific grant from funding agencies in the public, commercial, or not-for-profit sectors.

Author contributions

Chunlei Ju: Writing – review & editing, Writing – original draft, Methodology, Investigation, Formal analysis. Kai Yang: Writing – original draft, Supervision, Project administration, Methodology. Qingwei Yang: Validation, Methodology, Data curation. Chunhong Wang: Data curation. Yang Mi: Data curation. Hongming Ji: Supervision, Software, Resources, Project administration, Funding acquisition, Conceptualization.

Declarations

Competing interests

The authors declare no competing interests.

Additional information

Correspondence and requests for materials should be addressed to C.W. or H.J.

Reprints and permissions information is available at www.nature.com/reprints.

Publisher's note Springer Nature remains neutral with regard to jurisdictional claims in published maps and institutional affiliations.

Open Access This article is licensed under a Creative Commons Attribution-NonCommercial-NoDerivatives 4.0 International License, which permits any non-commercial use, sharing, distribution and reproduction in any medium or format, as long as you give appropriate credit to the original author(s) and the source, provide a link to the Creative Commons licence, and indicate if you modified the licensed material. You do not have permission under this licence to share adapted material derived from this article or parts of it. The images or other third party material in this article are included in the article's Creative Commons licence, unless indicated otherwise in a credit line to the material. If material is not included in the article's Creative Commons licence and your intended use is not permitted by statutory regulation or exceeds the permitted use, you will need to obtain permission directly from the copyright holder. To view a copy of this licence, visit http://creativecommons.org/licenses/by-nc-nd/4.0/.

© The Author(s) 2025